Theoretical model for slender FRP-confined circular RC columns

T. Jiang [1, 2] and J.G. Teng [1,*]

[1]Department of Civil and Structural Engineering
The Hong Kong Polytechnic University, Hong Kong, China
[2]Zhejiang Provincial Key Laboratory of Space Structures
Department of Civil Engineering
Zhejiang University, Hangzhou, Zhejiang Province, China
*cejgteng@polyu.edu.hk

Abstract: An important application of fiber-reinforced polymer (FRP) composites is to provide confinement to reinforced concrete (RC) columns to enhance their load-carrying capacity. However, this application is generally restricted to short columns as existing design guidelines do not contain provisions for the design of FRP jackets for slender columns. This situation has been due to both the scarcity of test data and the lack of rigorous theoretical studies into the behaviour of slender FRP-confined RC columns. This paper presents a theoretical model for slender FRP-confined circular RC columns based on the numerical integration method; Lam and Teng's stress-strain model is employed to describe the behaviour of FRP-confined concrete in the column. Predictions from the theoretical column model are compared with existing test results, which demonstrates that the theoretical model is reasonably accurate in reproducing the experimental results of FRP-confined circular RC columns. These comparisons also demonstrate the need to conduct careful tests on large-scale columns to eliminate some uncertainties associated with the existing test data to enable a more conclusive verification of the proposed theoretical column model.

Key words: FRP; confinement; concrete; slender columns; theoretical model

1 Introduction

The use of externally-bonded fibre-reinforced polymer (FRP) reinforcement for the strengthening of reinforced concrete (RC) structures has become a popular technology over the past decade. One of the important applications of the FRP strengthening technology is in the enhancement of RC column load-carrying capacity through the provision of confining FRP jackets (or wraps). The column jacketing technique is particularly effective for circular columns as the strength and ductility of concrete in a circular section can be substantially increased through lateral confinement.

To facilitate practical applications, various guidelines have been developed for the design of FRP systems for strengthening RC structures [1-6]. A significant deficiency of these guidelines is that all of them are only concerned with the design of FRP jackets for short columns with a negligible slenderness (i.e. second-order) effect; none of them includes any information on the design of FRP jackets for slender columns. Even for the safe application of the existing design provisions for short RC columns, there is a need to define a slenderness limit for short FRP-confined columns. Among the existing design guidelines, only the ISIS Canada guideline [2] provides such a

definition intended for short FRP-confined RC columns with no significant bending (i.e. concentric compression or slightly eccentric compression). The existing definitions for short RC columns cannot be used in the design of FRP-confined RC columns because FRP confinement leads to a greater slenderness effect in columns as has been demonstrated by the limited test results of FRP-confined circular RC columns [7-9]. This unsatisfactory situation has been due to both the scarcity of test data and the lack of theoretical studies into the behaviour of slender FRP-confined RC columns.

Against this background, this paper presents a theoretical model for slender FRP-confined circular RC columns. This theoretical column model incorporates Lam and Teng's stress-strain model [10] for FRP-confined concrete in circular columns with modifications as reported by Teng *et al.* [11] and is based on the numerical integration method [12]. The paper first briefly presents Lam and Teng's stress-strain model for FRP-confined concrete in circular columns and its application in section analysis of FRP-confined RC columns. The theoretical column model is next described in detail, followed by its verification using experimental results of both RC columns and FRP-confined circular RC columns. It should be noted that only a very limited number of tests on slender FRP-confined circular RC columns have been reported in the open literature [7-9] and all those available to the authors are used herein to verify the proposed model.

The authors' work on slender FRP-confined RC columns has been partially motivated by the need to formulate design provisions for the Chinese National Standard "Technical Code for Infrastructure Application of FRP Composites", which is currently being considered by the Ministry of Housing and Urban-Rural Development of China for official approval. This new Code has been developed within the framework of the current Chinese Code for Design of Concrete Structures [13]. Therefore, some of the considerations in the present study follow the specifications given in Ref. [13] and these considerations are highlighted where appropriate.

2   Lam and Teng's stress-strain model for FRP-confined concrete

2.1   Lam and Teng's Model

The original version of Lam and Teng's stress-strain model [10] has been adopted by both UK's Concrete Society design guideline [6] and the latest ACI guideline [4] for strengthening concrete structures. Lam and Teng's model adopts a simple form (a parabolic first portion which connects smoothly to a linear second portion) which automatically reduces to that for unconfined concrete when no FRP is provided. This simple form is described by the following expressions:

$$\sigma_c = E_c \varepsilon_c - \frac{\left(E_c - E_2\right)^2}{4 f_{co}^{'}} \varepsilon_c^2 \quad \text{for} \quad 0 \leq \varepsilon_c < \varepsilon_t \tag{1a}$$

$$\sigma_c = f_{co}^{'} + E_2 \varepsilon_c \quad \text{for} \quad \varepsilon_t \leq \varepsilon_c \leq \varepsilon_{cu} \tag{1b}$$

where σ_c and ε_c are the axial stress and the axial strain respectively, E_c is the elastic modulus of unconfined concrete, E_2 is the slope of the linear second portion, and $f_{co}^{'}$

is the compressive strength of unconfined concrete. The transition strain ε_t between the parabolic first portion and the linear second portion and the slope of the linear second portion E_2 are respectively given by:

$$\varepsilon_t = \frac{2f_{co}^{'}}{E_c - E_2} \tag{2}$$

$$E_2 = \frac{f_{cc}^{'} - f_{co}^{'}}{\varepsilon_{cu}} \tag{3}$$

where $f_{cc}^{'}$ and ε_{cu} are respectively the compressive strength and the ultimate axial strain of confined concrete. The expressions for $f_{cc}^{'}$ and ε_{cu} have been recently refined by Teng *et al.* [11] based on recent test results and an accurate analysis-oriented stress-strain model for FRP-confined concrete [14, 15]. These new expressions are given by:

$$\frac{f_{cc}^{'}}{f_{co}^{'}} = \begin{cases} 1 & \text{if } \rho_K < 0.01 \\ 1 + 3.5(\rho_K - 0.01)\rho_\varepsilon & \text{if } \rho_K \geq 0.01 \end{cases} \tag{4}$$

$$\frac{\varepsilon_{cu}}{\varepsilon_{co}} = 1.75 + 6.5\rho_K^{0.8}\rho_\varepsilon^{1.45} \tag{5}$$

where $\rho_K = E_{frp}t/(E_{seco}R)$ is the confinement stiffness ratio and $\rho_\varepsilon = \varepsilon_{h,rup}/\varepsilon_{co}$ is the strain ratio. It should be noted that the confinement ratio $f_l/f_{co}^{'}$ can be interpreted as a product of ρ_K and ρ_ε ($f_l/f_{co}^{'} = \rho_K\rho_\varepsilon$). Here, E_{frp} is the elastic modulus of FRP in the hoop direction, t is the thickness of the FRP jacket, $\varepsilon_{h,rup}$ is the hoop rupture strain of the FRP jacket, R is the radius of the confined concrete core, E_{seco} and ε_{co} are the secant modulus and the axial strain at the compressive strength of unconfined concrete, with $E_{seco} = f_{co}^{'}/\varepsilon_{co}$. When this model is used in a design specification, the model may need small adjustments so that the curve reduces to that for unconfined concrete in a specific national code. In Ref. [13], normal strength concrete is assumed to have $\varepsilon_{co} = 0.002$ and an ultimate axial strain of 0.0033. As a result, $E_c = 1000f_{co}^{'}$ and the original value of 1.75 for the first term on the right hand side of Eq. 5 is replaced by 1.65 in the present study, so that the stress-strain model for FRP-confined concrete reduces to that for unconfined normal strength concrete given in Ref. [13] when no FRP is provided. It should be noted that the refined version of Lam and Teng's stress-strain model with the above two adjustments was used in all the calculations reported in the present paper. For brevity, this refined version is still referred to simply as Lam and Teng's model in the remainder of the paper.

2.2 Section analysis using Lam and Teng's model

Lam and Teng's model is based on concentric compression tests of FRP-confined concrete, but in a column under combined bending and axial compression, a strain gradient exists. In section analysis of conventional RC columns, the assumption that

the stress-strain curve of concrete in an eccentrically-loaded column is the same as that of concrete under concentric compression is widely used. For FRP-confined RC columns, whether the same assumption is equally acceptable is not yet completely clear. The few existing studies on the behaviour of eccentrically-loaded circular columns with FRP confinement [7, 16, 17] have not provided a clear understanding of the issue. Based on the information available to date, it seems reasonable at this stage to adopt this assumption in the analysis of FRP-confined circular RC sections as has been done by previous researchers [18-24].

When the stress-strain curve of FRP-confined concrete subjected to concentric compression is directly used in a section analysis, the analysis procedure is similar to that for conventional RC columns. The only difference in the analysis procedure introduced by the presence of FRP confinement is the use of a different concrete stress-strain relationship that considers the confinement effect of the FRP. Numerical integration over the section can still be carried out using the layer method in which the column section is divided into many small horizontal layers as shown in Fig. 1. Full composite action between concrete and FRP is assumed. Compressive stresses are taken to be positive and the tensile strength of concrete is ignored. Plane sections are assumed to remain plane. Any confinement effect from the hoop steel reinforcement is ignored, so the present theoretical column model is applicable only to columns with very limited transverse steel reinforcement. The longitudinal steel reinforcement is assumed to have an elastic-perfectly plastic stress-strain curve. The axial load N and the bending moment M at any stage of loading carried by the section with the reference axis going through the centre of the section are found by integrating the stresses over the section:

$$N = \int_{\lambda_c = R - x_n}^{R} \sigma_c b_c \left(d\lambda_c \right) + \sum_{i=1}^{n} \left(\sigma_{si} - \sigma_c \right) A_{si} \tag{6a}$$

$$M = \int_{\lambda_c = R - x_n}^{R} \sigma_c b_c \lambda_c \left(d\lambda_c \right) + \sum_{i=1}^{n} \left(\sigma_{si} - \sigma_c \right) A_{si} \left(R - d_{si} \right) \tag{6b}$$

where R is the radius of the section, b_c is the width of the section at a distance λ_c from the reference axis, x_n is the depth of the neutral axis, σ_{si} is the stress in the ith layer of longitudinal steel reinforcement, d_{si} is the corresponding distance from the reference axis, and A_{si} is the corresponding cross-sectional area. The stress of concrete σ_c in the compression zone can be determined from Eq. 1. σ_{si} can be calculated from:

$$\sigma_{si} = E_s \varepsilon_{si} \quad \text{if } \left| \varepsilon_{si} \right| < \frac{f_y}{E_s} \tag{7a}$$

$$\sigma_{si} = \frac{\varepsilon_{si}}{\left| \varepsilon_{si} \right|} f_y \quad \text{if } \left| \varepsilon_{si} \right| \geq \frac{f_y}{E_s} \tag{7b}$$

where E_s and f_y are the elastic modulus and the yield strength of the longitudinal steel reinforcement respectively. Eq. 6 is applicable at any stage of loading. The

ultimate limit state of the column is reached when the strain at the extreme concrete compression fiber reaches the ultimate axial strain of FRP-confined concrete, signifying crushing of concrete due to FRP hoop tensile rupture. This ultimate axial strain is defined by Eq. 5 with the original value of 1.75 for the first term on the right hand side replaced by 1.65.

3 Theoretical model for slender FRP-confined RC columns

3.1 General

The method of analysis used herein is the well-known numerical integration method. This method was originally proposed by Newmark [12] and has been widely adopted in the analysis of RC columns [*e.g.* 25, 26], steel columns [*e.g.* 27] and composite columns [*e.g.* 28, 29]. In this study, this method is applied to pin-ended FRP-confined circular RC columns subjected to eccentric loads at both ends with the end eccentricities being e_1 and e_2, respectively (Fig. 2). It should be noted that e_2 is taken to be the one with a larger absolute value and is always assigned a non-negative value. This means that e_1 has a negative value when the column is bent in double curvature. The column with a length l is equally divided into a desirable number of segments each with a length of Δl. The column section at each grid point is divided into a desirable number of layers parallel to the neutral axis. The lateral displacement at each grid point at a particular loading stage is sought in an iterative manner by making use of the axial load-moment-curvature ($N - M - \phi$) relationship of the column section and the numerical integration function of the column. The full-range axial load-lateral deflection curve of the column (referred to as the load-deflection curve for brevity hereafter) can then be traced in an incremental manner using either a force-control or deflection-control technique. For the ascending branch of the load-deflection curve, it is more convenient to use the force-control technique (increasing the axial load by small steps). In the case of a stability failure, a descending branch of the load-deflection curve exists and the deflection-control technique (increasing the deflection of a particular grid point by small steps) should be used to trace the descending branch. In summary, the axial load-moment-curvature relationship and the numerical integration function are the two key elements of the numerical integration method and they are discussed in detail in the following sub-sections, where the procedure for generating the full-range load-deflection curve is also described.

3.2 Axial load-moment-curvature relationship

For a given column section, there exists a unique moment-curvature curve under a particular axial load N. This moment-curvature curve can be readily constructed using the section analysis approach described in the preceding section. For a given axial load N, the corresponding moment-curvature curve can be generated by specifying a series of suitable strain values for the extreme compression fiber of concrete ε_{cf} up to its ultimate value ε_{cu}. For each strain value, the depth of the neutral axis x_n is varied until the resultant axial force acting on the section, calculated from Eq. 6a, equals the applied axial load. Once the neutral axis position has been

determined, the moment can be evaluated using Eq. 6b and the curvature can be calculated using the following expression:

$$\phi = \frac{\varepsilon_{cf}}{x_n}$$

(8)

In the present study, every section was divided into 50 horizontal layers. The solution process can be taken to have been successfully completed once the difference between the resultant axial force and the applied axial load is very small (*e.g.* within 0.1%); in the calculations of the present study, a column axial force difference of $10^{-6} N$ was adopted as the convergence criterion. Each moment-curvature curve in the present study was constructed from 200 equal-curvature segments.

3.3   Numerical integration for the column deflection

Since the lateral deflection of the column is very small compared to the length of the column, the curvature can be taken to be the second order derivative of the lateral deflection of the column. Using the central difference equation, the relationship between the lateral deflection and the curvature can be expressed as:

$$\frac{f_{(i+1)} - 2f_{(i)} + f_{(i-1)}}{(\Delta l)^2} = -\phi_{(i)}$$

(9)

where $f_{(i)}$ and $\phi_{(i)}$ are the lateral deflection and the curvature at the ith grid point respectively and $i = 2,3,\cdots m-1$. i is the index of the grid point and $m-1$ is the number of segments that the column is equally divided into (Fig. 2). $m = 31$ was used in the present study. Eq. 9 can be rewritten as:

$$f_{(i+1)} = 2f_{(i)} - f_{(i-1)} - \phi_{(i)}(\Delta l)^2$$

(10)

Eq. 10 is the numerical integration function used to find the lateral deflection of the column. The implementation of this equation is described in the following section.

3.4   Generation of the ascending branch of the load-deflection curve

The axial load is increased by small increments to generate the ascending branch of the load-deflection curve. For a given axial load N, the first step is to construct the corresponding moment-curvature curve using the procedure described above. Under this axial load, the first order moment at each grid point can be easily calculated as:

$$M_{1,(i)} = N \cdot e_{(i)}$$

(11)

where $M_{1,(i)}$ and $e_{(i)}$ are the first order moment and the initial eccentricity at the ith grid point respectively. Note that the initial eccentricity follows a linear distribution

with $e_{(1)} = e_2$ and $e_{(m)} = e_1$. If the lateral deflection of the column is known, the second order moment can be expressed as:

$$M_{2,(i)} = N \cdot f_{(i)} \tag{12}$$

and the total moment is then given by:

$$M_{(i)} = M_{1,(i)} + M_{2,(i)} = N \cdot \left(e_{(i)} + f_{(i)} \right) \tag{13}$$

A value for $f_{(2)}$ needs to be assumed for the analysis to proceed to the next step. The assumed value can be any reasonably small value or simply zero. The moment at this grid point $M_{(2)}$ can then be evaluated using Eq. 13 and the curvature at this grid point $\phi_{(2)}$ can be retrieved from the moment-curvature curve corresponding to the present axial load using linear interpolations. With $M_{(2)}$ and $\phi_{(2)}$ known and noting that $f_{(1)} = 0$, the lateral displacement of the third grid point $f_{(3)}$ can be evaluated using Eq. 10. It is evident that the lateral deflection of a column can be traced from grid point to grid point by repeating the above procedure. Once the calculations eventually reach the other end of the column, its lateral displacement needs to be examined to see if it satisfies $f_{(m)} = 0$. If this condition is satisfied, then the correct lateral deflection of the column is found. Otherwise, the assumed value of $f_{(2)}$ needs to be adjusted until $f_{(m)} = 0$ is satisfied. It is convenient to select the new value of $f_{(2)}$ to be equal to the previous $f_{(2)}$ value minus $\dfrac{f_{(m)}}{m-1}$ [27]. In the present study, the solution was considered to be acceptable if the calculated $f_{(m)}$ reached an absolute value smaller than 10^{-4} mm.

The above procedure determines the lateral deflection of a column under a particular axial load. The ascending branch of the load-deflection curve can be obtained by calculating the deflection of the column for a series of successively increasing loads. In the present study, an initial load increment (i.e. load step size) of $0.1N_{u1}$ was used, where N_{u1} is the axial load capacity of the column section under consideration when subjected to concentric compression as given by:

$$N_{u1} = f'_{cc} A_c + f_y A_s \tag{14}$$

where A_c and A_s are the total cross-sectional areas of concrete and longitudinal steel reinforcement, respectively. After a series of load increments, the applied load eventually exceeds the maximum load that the column can sustain. This situation arises when the moment at any grid point calculated by Eq. 13 exceeds the maximum moment on the moment-curvature curve under the present axial load. When this occurs, the calculation process needs to restart from the last load level and a smaller load increment of $0.01N_{u1}$ is used for the subsequent load steps. After some steps, a similar treatment needs to be adopted with the load step size reduced by a factor of 10.

The same process is repeated until the load step size is eventually reduced to $10^{-6} N_{u1}$. The axial load capacity of the column N_u is then taken to be the maximum load for which a convergent solution of the lateral deflection can be found. The corresponding value of $f_{(2)}$ is recorded as a reference displacement value f_{ref} for use in the generation of the descending branch of the load-deflection curve, as discussed in the following sub-section.

3.5   Generation of the descending branch of the load-deflection curve

If a column is controlled by material failure, its load-deflection curve has no descending branch. However, if a column is slender enough to trigger stability failure, a descending branch of the load-deflection curve exists. In this case, the displacement-control technique should be used to trace the descending branch. The numerical procedure is similar to that described in the previous sub-section with the only difference being that the aim is to find the correct axial load under a prescribed value of $f_{(2)}$.

A displacement increment of $0.1 f_{ref}$ is initially used (i.e. the prescribed value of $f_{(2)}$ in the first step is $1.1 f_{ref}$). The initial assumed value of the corresponding axial load can be taken as N_u. The corresponding deflected configuration can then be calculated using the numerical procedure described in the previous sub-section. It should be noted that the calculated $f_{(m)}$ always has a negative value, because the actual axial load must be smaller than N_u. The assumed axial load is thus successively reduced at steps of $0.01 N_u$ until the calculated $f_{(m)}$ has a positive value. The correct axial load can then be determined using the bisection method by setting the last two assumed values of axial load to be the upper bound and the lower bound respectively in the bisection method. The final axial load derived from the bisection method is the solution for the current step and is used as the initial value in the next step. After a series of increments of $f_{(2)}$, the analysis eventually fails to find a convergent solution. This situation arises when the moment at any grid point calculated by Eq. 13 exceeds the maximum moment on the moment-curvature curve under the present axial load. When this occurs, the calculation needs to restart from the previous prescribed value of $f_{(2)}$ and with a smaller displacement increment of $0.01 f_{ref}$. The entire process is repeated and the analysis stops when the increment is reduced to $10^{-6} f_{ref}$.

It should be noted that the accuracy of the present analysis is affected by a number of factors (i.e. the number of segments the column is divided into, the number of horizontal layers the cross section is divided into, the number of segments the moment-curvature curve consists of, and the tolerances adopted in the analysis). A convergence study showed that all these factors have been very well looked after in the present study (i.e. any refinement to these factors will not have any significant effect on the numerical results). A computer program was developed to implement the numerical procedure described above using Matlab 7.1.

4 Numerical comparison for RC columns

4.1 Comparison with Cranston's numerical results

The accuracy of the present theoretical model and its numerical implementation is first verified using the numerical results of Cranston's theoretical model [26] for RC columns, which was based on a similar numerical integration procedure. Cranston's model [26] used the same stress-strain relationships for both concrete and steel as are adopted by the present theoretical column model except that the concrete was assumed to have an ultimate axial strain of 0.0035 in the former. This value was also used in the present model for this set of comparisons. Table 1 lists the properties of the columns analyzed by Cranston [26]. These columns were all pin-ended and were eccentrically loaded at only one end. The cross-sectional shape was rectangular rather than circular and is illustrated in Fig. 3. The height and the width of the cross section are denoted by h and b respectively and the eccentricity is in the height direction. The steel reinforcement ratio is denoted by ρ_s and the distance between the top and the bottom layers of the steel reinforcement is denoted by h'. f_{cu} is the characteristic cube strength of concrete and $f_{y,k}$ is the characteristic yield strength of steel reinforcement. Cranston [26] normalized the load-deflection curves (Fig. 4) using appropriate reference values. The lateral deflection at mid-height of the column f_{mid} was normalized by the section height while the axial load was normalized by the design value of the section axial load capacity under concentric compression N_{uo}, which was determined from the design values of material strengths (the numbers bracketed in Table 1; the partial safety factors for concrete and steel are 1.5 and 1.15 respectively). However, the characteristic material strengths were used in the numerical analyses. The predictions of both models are shown in Fig. 4. It can be clearly seen that these predictions are in excellent agreement for both the material failure and stability failure cases.

4.2 Comparison with Kim and Yang's experimental results

Predictions of the present theoretical model are also compared with Kim and Yang's test results for RC columns [30]. Details of Kim and Yang's tests are given in Table 2. These specimens were square in shape and had a wide range of concrete strength. All these specimens were bent in symmetrical single curvature ($e_1 = e_2$). In these tests, two physically identical columns were prepared for each configuration. Close agreement between the present predictions and the test results can be seen in the last column of Table 2. In addition, the full-range load-deflection curves were also reported by Kim and Yang [30], and those of the normal strength series are compared with predictions of the present model in Fig. 5. No further comparisons for RC columns are discussed herein because the present method of analysis has long been well-accepted for RC columns [25, 26].

5 Numerical comparison for FRP-confined RC columns

5.1 General

The small number of experimental studies on slender FRP-confined circular RC columns have been carried out by Ranger and Bisby [7], Fitzwilliam and Bisby [8], Tao *et al.* [9], and Hadi [17]. Hadi [17] tested five small-scale (150 mm in diameter) circular normal strength concrete columns wrapped with CFRP and subjected to axial loading with the same end eccentricity of 42.5 mm. One reference column which received no FRP wrapping was also tested. Four of the five FRP-confined columns were not provided with internal steel reinforcement so they failed by tensile cracking of concrete. Unfortunately, the hoop strains on the FRP jacket were not reported which makes it difficult for these test results to be used to verify the proposed theoretical column model.

5.2   Columns tested by Fitzwilliam and Bisby and Ranger and Bisby

The two column test series of Ranger and Bisby [7] and Fitzwilliam and Bisby [8] were conducted by the same research group and the test configurations of the two series are similar. Therefore, these two test series are discussed together, although they had different test objectives. Ranger and Bisby [7] varied the load eccentricity but fixed the column height while Fitzwilliam and Bisby [8] varied the column height but fixed the load eccentricity. In Ranger and Bisby's test series [7], all the columns were 152mm in diameter and 600 mm in height, and were connected to a steel system at both column ends to create the pinned end condition and the needed load eccentricity. All the columns were reinforced with four 6.4 mm diameter steel bars longitudinally and 6.4 mm diameter steel ties spaced at 100 mm transversely with a 25 mm concrete cover to the longitudinal reinforcement. A total of six load eccentricities were considered: 0, 5, 10, 20, 30, or 40 mm. For each load eccentricity, a column confined with a single ply of CFRP as well as an unconfined reference column was tested. The FRP jacket included a 100 mm overlapping zone with its centerline being at the theoretically least compressed point around the circumference. The concrete had a cylinder strength of 33.2 MPa, the steel reinforcement had a yield strength of 710 MPa [31], and the FRP had an elastic modulus of 90 GPa (based on a nominal thickness of 0.381 mm) and a rupture strain of 1.12% obtained from tensile coupon tests. A summary of Ranger and Bisby's tests [7] is given in Table 3.

In Fitzwilliam and Bisby's test series [8], the column height varied from 300 mm to 1200 mm at an interval of 300 mm and all the columns were tested with a fixed load eccentricity of 20 mm. The steel reinforcement and the FRP used in the study were the same as those used in Ranger and Bisby [7]. The concrete cylinder strength averaged from three batches of cylinder tests conducted during the period of column tests was 35.5 MPa [31]. The other test parameters were similar to those of Ranger and Bisby's tests [7]. It should be noted that some columns received longitudinal FRP wrapping before hoop FRP wrapping, but these tests have been excluded from the present comparison. Fitzwilliam and Bisby's tests [8] are summarized in Table 4. In both test series, the lateral deflection of the column was monitored at three different vertical locations with one being located at the mid-height of the column.

Auxiliary tests on standard FRP-confined concrete cylinders under concentric compression were also conducted for both test series. The concrete cylinders were made from the same concrete and confined with the same type and amount of FRP as the columns. These cylinder tests are summarized in Table 5. The concrete cylinders in Ranger and Bisby's study [7] were only confined with a 1-ply CFRP jacket while

some of the cylinders in Fitzwilliam and Bisby's study [8] were confined with a 2-ply CFRP jacket because some of the columns tested by Fitzwilliam and Bisby [8] were also confined with a 2-ply CFRP jacket. The compressive strength of unconfined concrete varied slightly in Fitzwilliam and Bisby's tests [8] because the concrete cylinders were tested at different ages during column testing. It should be noted that in Ref. [7], the FRP hoop rupture strain found from their FRP-confined cylinder tests is reported to be 0.62%, a much smaller value than that found from Fitzwilliam and Bisby's FRP-confined cylinder tests [8] (1.17% [31]), although the test configurations were almost the same in the two test series. It was later confirmed [31] that this small value arose from an editorial error and the correct value is 1.15%. The compressive strength f_{cc}' and the ultimate axial strain ε_{cu} for these FRP-confined cylinders predicted by Lam and Teng's model are listed in the last two columns of Table 5. It can be seen that the predicted values of the compressive strength are reasonably close to the experimental values, however, the predicted values of the ultimate axial strain are much larger than the experimental values, particularly for the specimens confined with a 1-ply FRP jacket. To minimize the errors that might arise from this discrepancy in modeling the column behaviour, the experimental values of f_{cc}' and ε_{cu} were directly incorporated in Lam and Teng's model in predicting the behaviour of test columns. $f_{cc}' = 44.2\,\text{MPa}$ and $\varepsilon_{cu} = 0.86\%$ were used in modelling the columns tested by Ranger and Bisby [7]. For the columns tested by Fitzwilliam and Bisby [8], $f_{cc}' = 40.7\,\text{MPa}$ and $\varepsilon_{cu} = 0.788\%$ were used for the 1-ply jacket while $f_{cc}' = 60.1$ and $\varepsilon_{cu} = 1.443\%$ were used for the 2-ply jacket. However, the predicted values of f_{cc}' and ε_{cu} were also used in predicting the behaviour of test columns to produce another set of results for comparison.

The predicted axial load capacities of all columns are compared with the experimental values in Tables 3 and 4. It can be noted that for all the unconfined columns in Ranger and Bisby's study [7], their axial load capacities are overestimated by the theoretical model by some 20% while this overestimation is much smaller for Fitzwilliam and Bisby's tests [8]. The relatively large overestimation observed for Ranger and Bisby's tests [7] may be due to the following factors in the tests: 1) additional eccentricities due to geometric/material imperfections and inaccurate alignment of load; and 2) spalling of the concrete cover in unconfined columns during testing which reduces the effective cross-sectional area. In particular, it can be shown that the theoretical results are sensitive to an additional eccentricity, especially when the nominal load eccentricity is small. For example, if a 10 mm additional eccentricity is assumed, then the predicted axial load capacity of column U-0 becomes 525 kN, which is much closer to the experimental value. However, in the comparisons for these two test series, no additional eccentricity was used except for columns U-0 and C-0 (subjected to nominally concentric compression) where a small eccentricity of 1 mm was used. For a column subjected to concentric compression, a small load eccentricity (or other forms of imperfection) needs to be introduced into the theoretical model as otherwise no lateral deflections can be predicted by the theoretical model. For the FRP-confined columns, in most cases, their axial load capacity is underestimated by about 5% to 15%. The only exceptions occurred for columns C-30 and C-40 which had relatively large load eccentricities. Their axial load capacities are overestimated by nearly 20%. While these underestimations might be interpreted as being due to the unfavorable effect of load eccentricity on confinement effectiveness, such an interpretation

requires more evidence because: 1) such a trend cannot be identified from the results for the smaller load eccentricities (0, 5, 10, 15, 20 mm); 2) the theoretical predictions are sensitive to an additional eccentricity whose exact value is unknown; and 3) experimental scatters are likely to exist in these test results.

The theoretical and experimental full-range load-deflection curves of FRP-confined columns tested by Ranger and Bisby [7] and Fitzwilliam and Bisby [8] are compared in Figs 6 and 7 respectively. Two theoretical curves are shown for each column; they were produced using the experimental and the predicted f'_{cc} and ε_{cu} values respectively. All the theoretical curves terminate when the extreme compression fiber reaches the ultimate axial strain of confined concrete. It should be noted that column C-0 in Ranger and Bisby's test series [7] and the pair of physically identical columns 300C-1-0A and 300C-1-0B in Fitzwilliam and Bisby's test series [8] have been excluded from the present comparisons, because only very small lateral deflections of these columns were recorded. This is due to the fact that the former had a relatively small height-to-diameter ratio of four and was tested under nominally concentric compression while the latter only had a length-to-diameter ratio of two, so the slenderness effect in these columns was not significant enough to induce significant lateral deflections. It can be seen in Figs 6 and 7 that for the same column, the theoretical curve produced using the f'_{cc} and ε_{cu} values predicted by Lam and Teng's model terminates at a larger deformation value, which is closer to test results, than the other theoretical curve. This is because the prediction of the deformation capacity of these columns largely depends on the value used for the ultimate axial strain of confined concrete; this value from Lam and Teng' stress-strain model is significantly larger than that from the FRP-confined cylinder tests (see Table 5). This observation also implies that the load eccentricity might have an effect on the stress-strain behaviour of FRP-confined concrete (*e.g.* increasing the ultimate axial strain of FRP-confined concrete) and this possible effect needs to be fully clarified in the future. It can also be seen in Figs 6 and 7 that there exist considerable discrepancies between the theoretical and the experimental values of column stiffness. This may be due to inaccurate displacement measurements at the initial loading stage because the lateral deflections might have been too small to be precisely measured (it is worth noting that even some negative lateral displacements at the mid-height of column C-5 were recorded). It should also be noted that the lateral displacements of column C-10 were not accurate (see Fig. 6b), as confirmed later [31]. Fig. 6b shows that column C-10 possessed a much larger deformation capacity than column C-20. This contradicts engineering intuition, because column C-20 should have a larger deformation capacity than column C-10, as the former was loaded with a larger initial load eccentricity and both columns failed at similar hoop rupture strains of the FRP jacket (1.07% for column C-10 and 1.15% for column C-20).

5.3   Column tests by Tao *et al.*

Tests on slender FRP-confined circular RC columns performed by Tao *et al.* [9] have also been analyzed using the present theoretical model. A total of 16 columns were tested and the properties of these columns are listed in Table 6. All the columns were 150mm in diameter and reinforced with four 12 mm longitudinal steel bars and 6 mm steel ties spaced at 100 mm. The columns had a 21 mm concrete cover to the longitudinal steel reinforcement. The C1 series had a column height-to-diameter ratio

of 8.4 while this ratio for the C2 series was 20.4. Each series included four different load eccentricities (0, 50, 100 and 150 mm) and for each eccentricity, one unconfined column and one FRP-confined column were tested. As the load eccentricities adopted were relatively large, all the columns were cast with corbel ends and capped with a steel plate with V-shaped grooves to achieve the required load eccentricities and a pinned end condition. A 150 mm overlapping zone was adopted in forming the FRP jacket and the position of the overlapping zone is similar to that adopted by Ranger and Bisby [7].

The average cylinder compressive strength of unconfined concrete was found from six standard concrete cylinders to be 48.2 MPa. The longitudinal steel reinforcement had a yield strength of 388.7 MPa. The CFRP had an elastic modulus of 255 GPa based on a nominal thickness of 0.17 mm per ply and a rupture strain of 1.67% based on tensile coupon tests. Three auxiliary FRP-confined concrete cylinders were tested under concentric compression to determine the stress-strain behaviour of FRP-confined concrete. These cylinders were confined with the same type and amount of FRP (2 plies of CFRP) as the columns. The stress-strain curves predicted using Lam and Teng's model are compared with the experimental curves of the FRP-confined cylinders in Fig. 8. It should be noted that only two experimental curves are shown in Fig. 8 because the third specimen experienced an unexpected experimental error during testing. The hoop rupture strain averaged from the two cylinders is 1.32% and this value was used when generating the predicted stress-strain curve. It can be seen that the predicted and experimental curves are in close agreement so Lam and Teng's model was directly used in the theoretical column model for the modeling of these columns.

The predicted axial load capacities of all columns are listed in Table 6. Again, a small eccentricity of 1 mm was used when analyzing columns tested under nominally concentric compression (i.e., columns C1-1U, C1-1R, C2-1U, and C2-1R). It is important to note that for all the unconfined columns, the predicted axial load capacity is considerably larger than the experimental value, particularly for those columns subjected to nominally concentric loading. By contrast, the predictions for FRP-confined columns are much more reasonable although the theoretical column model still leads to overestimations. This might be due to the same reasons as given earlier: additional eccentricities from geometric/material imperfections, inaccurate alignment of load, and the possible spalling of the concrete cover in unconfined columns. In an internal report [32] by the same research group, it was suggested that an additional eccentricity of 15 mm be used for unconfined columns and an additional eccentricity of 7.5 mm be used for FRP-confined columns when modelling Tao *et al.*'s column tests [9]. When this suggestion is adopted, the predicted values (bracketed in Table 6) become much closer to the experimental values. With the inclusion of the additional eccentricity in the theoretical column model, the average $N_{u,theo}/N_{u,test}$ ratio for the six FRP-confined columns with a non-zero nominal load eccentricity decreases from 1.11 to 1.01. However, the corresponding ratio for unconfined columns is still 1.19, indicating significant overestimation.

Another point worth noting is that the theoretical column model only predicts a marginal increase in the axial load capacity due to FRP wrapping, which is particularly true for series C2. This observation indicates that the effectiveness of FRP confinement decreases as columns become more slender. The same trend can also be

observed in the predictions for Fitzwilliam and Bisby's tests [8]. This is because FRP confinement can substantially increase the axial load capacity of an RC section, but the flexural rigidity of such a section in the range of confinement-enhanced resistance is much lower than its initial flexural rigidity.

The theoretical and experimental full-range load-deflection curves of the FRP-confined columns tested by Tao *et al.* [9] are also compared (Fig. 9). An additional eccentricity of 7.5 mm was added to the nominal load eccentricity when producing the theoretical curves shown in Fig. 9. For specimens C1-1R and C2-1R, two theoretical curves are shown. The upper one is for an additional eccentricity of 7.5 mm while the lower one is for an additional eccentricity of 15 mm. These two specimens were tested under nominally concentric compression, so their behaviour is more sensitive to the additional eccentricity. It can be seen that the use of a 15 mm additional eccentricity produced closer predictions, but the curves for a 7.5 mm additional eccentricity are also reasonably close to the experimental curves.

6 Conclusions

This paper has been concerned with the development and verification of a theoretical model for slender FRP-confined RC columns. This theoretical column model incorporates Lam and Teng's stress-strain model for FRP-confined concrete [10] as refined by Teng *et al.* [11] at the section behaviour level and finds the lateral deflection of a column through numerical integration at the column behaviour level. The predictions of the theoretical column model have been compared with experimental results of FRP-confined RC columns reported in the open literature. The comparisons and discussions presented in this paper allow the following conclusions to be drawn:

1) The numerical integration method has long been successfully used to model slender steel columns, RC columns and steel-concrete composite columns. However, to the best knowledge of the authors, the work presented in this paper represents the first application of the numerical integration method to the analysis of slender FRP-confined RC columns.

2) Numerical predictions of the proposed theoretical model have been shown to compare well with existing theoretical and experimental results of slender RC columns, demonstrating that the numerical integration method was correctly implemented.

3) Comparisons of predictions from the theoretical column model and existing test results for slender FRP-confined circular RC columns have shown that the proposed theoretical model is reasonably accurate in predicting the axial load capacity, but significant uncertainty exists in these comparisons as the test columns were small so the test results are believed to have been significantly influenced by unintended load eccentricities. There is a genuine need to conduct tests on larger-scale columns for a more reliable verification of the proposed theoretical column model.

4) Compared with the predictions for the axial load capacity, larger discrepancies exist between predictions of the proposed model and test results for the deformation capacity of slender FRP-confined RC columns. One possible reason is that the load eccentricity has a significant effect on the ultimate axial strain of FRP-confined concrete in an FRP-confined RC column, which is the key to the prediction of deformation capacity. More research is needed to clarify this issue, including the testing of larger-scale columns.

5) The numerical results have confirmed the experimental observation that the effectiveness of FRP confinement in enhancing the load-carrying capacity of a column decreases as the column becomes more slender. This is because FRP confinement can substantially increase the axial load capacity of an RC section, but the flexural rigidity of such a section in the range of confinement-enhanced resistance is much lower than its initial flexural rigidity.

6) This paper has been limited to slender FRP-confined circular RC columns, but the method of analysis can be easily extended to slender FRP-confined RC columns of other section forms if an accurate stress-strain model for FRP-confined concrete in a particular section form is available.

Acknowledgements

References

[1] fib. *Externally Bonded FRP Reinforcement for RC Structures*, The International Federation for Structural Concrete, Lausanne, Switzerland; 2001.

[2] ISIS. *Design Manual No. 4: Strengthening Reinforced Concrete Structures with Externally-Bonded Fibre Reinforced Polymers*, ISIS Canada; 2001.

[3] ACI-440.2R. *Guide for the Design and Construction of Externally Bonded FRP Systems for Strengthening Concrete Structures*, American Concrete Institute, Farmington Hills, Michigan, USA; 2002.

[4] ACI-440.2R. *Guide for the Design and Construction of Externally Bonded FRP Systems for Strengthening Concrete Structures*, American Concrete Institute, Farmington Hills, Michigan, USA; 2008.

[5] CNR-DT200. *Guide for the Design and Construction of Externally Bonded FRP Systems for Strengthening Existing Structures*, Advisory Committee on Technical Recommendations for Construction, National Research Council, Rome, Italy; 2004.

[6] Concrete Society. *Design Guidance for Strengthening Concrete Structures with Fibre Composite Materials*, Second Edition, Concrete Society Technical Report No. 55, Crowthorne, Berkshire, UK; 2004.

[7] Ranger, M. and Bisby, L.A. "Effects of load eccentricities on circular FRP-confined reinforced concrete columns", *Proceedings, 8th International Symposium on Fiber Reinforced Polymer Reinforcement for Concrete Structures (FRPRCS-8)*, University of Patras, Patras, Greece; 16-18 July 2007.

[8] Fitzwilliam, J. and Bisby, L.A. "Slenderness effects on circular FRP-wrapped reinforced concrete columns", *Proceedings, 3rd International Conference on FRP Composites in Civil Engineering*, Miami, Florida, USA, 13-15 December 2006; 499-502.

[9] Tao, Z., Teng, J.G., Han, L.H. and Lam, L. "Experimental behaviour of FRP-confined slender RC columns under eccentric loading", *Proceedings, Second International Conference on Advanced Polymer Composites for Structural Applications in Construction*, University of Surrey, Guildford, UK, 2004; 203-212.

[10] Lam, L. and Teng, J.G. "Design-oriented stress-strain model for FRP-confined concrete", *Construction and Building Materials*, 2003; 17 (6-7): 471-489.

[11] Teng, J.G., Jiang, T., Lam, L. and Luo, Y.Z. "Refinement of a design-oriented stress-strain model for FRP-confined concrete", *Journal of Composite for Construction*, ASCE, 2009; 13(4): 269-278.

[12] Newmark, N.M. "Numerical procedure for computing deflections, moments, and buckling loads", ASCE *Transactions*, 1943; 108: 1161-1234.

[13] GB-50010. *Code for Design of Concrete Structures*, China Architecture and Building Press, China; 2002.

[14] Teng, J.G., Huang, Y.L. Lam. L and Ye L.P. "Theoretical model for fiber reinforced polymer-confined concrete", *Journal of Composites for Construction*, ASCE, 2007; 11(2): 201-210.

[15] Jiang, T. and Teng, J.G. "Analysis-oriented models for FRP-confined concrete: a comparative assessment", *Engineering Structures*, 2007; 29(11): 2968-2986.

[16] Fam, A., Flisak, B. and Rizkalla, S. "Experimental and analytical modeling of concrete-filled fiber-reinforced polymer tubes subjected to combined bending and axial loads", *ACI Structural Journal*, 2003; 100(4): 499-509.

[17] Hadi, M.N.S. "Behaviour of wrapped normal strength concrete columns under eccentric loading", *Composite Structures*, 2006; 72(4): 503-511.

[18] Saadatmanesh, H., Ehsani, M.R. and Li, M.W. "Strength and ductility of concrete columns externally reinforced with fiber composites straps", *ACI Structural Journal*, 1994; 91(4): 434-447.

[19] Monti, G., Nistico, N. and Santini, S. "Design of FRP jackets for upgrade of circular bridge piers", *Journal of Composites for Construction*, ASCE, 2001; 5(2): 94-101.

[20] Yuan, W. and Mirmiran, A. "Buckling analysis of concrete-filled FRP tubes", *International Journal of Structural Stability and Dynamics,* 2001; 1(3): 367-383.

[21] Cheng, H.L., Sotelino, E.D. and Chen, W.F. "Strength estimation for FRP wrapped reinforced concrete columns", *Steel and Composite Structures*, 2002; 2(1): 1-20.

[22] Teng, J.G., Chen, J.F., Smith, S.T. and Lam. L. *FRP-Strengthened RC Structures*, John Wiley and Sons, Inc., UK; 2002.

[23] Binici, B. "Design of FRPs in circular bridge column retrofits for ductility enhancement", *Engineering Structures*, 2008; 30(3): 766-776.

[24] Yuan, X.F., Xia, S.H., Lam, L. and Smith, S.T. "Analysis and behaviour of FRP-confined short concrete columns subjected to eccentric loading", *Journal of Zhejiang University Science A*, 2008; 9(1): 38-49.

[25] Pfrang, E.O. and Siess, C.P. "Analytical study of the behavior of long restrained reinforced concrete columns subjected to eccentric loads", *Structural Research Series,* No. 214, University of Illinois, Urbana, Illinos; 1961.

[26] Cranston, W.B. *Analysis and Design of Reinforced Concrete Columns*, Research Report 20, Cement and Concrete Association, UK; 1972.

[27] Shen, Z.Y. and Lu, L.W. "Analysis of initially crooked, end restrained steel columns", *Journal of Constructional Steel Research*, 1983; 3(1): 10-18.

[28] Choo, C.C., Harik, I.E. and Gesund, H. "Strength of rectangular concrete columns reinforced with fiber-reinforced polymer bars", *ACI Structural Journal*, 2006; 103(3): 452-459.

[29] Tikka, T.M. and Mirza, S.A. "Nonlinear equation for flexural stiffness of slender composite columns in major axis bending", *Journal of Structural Engineering*, ASCE, 2006; 132(3): 387-399.

[30] Kim, J.K. and Yang, J.K. "Buckling behaviour of slender high-strength concrete columns", *Engineering Structures*, 1995; 17(1): 39-51.

[31] Bisby, L.A. Private communication; 2008.

[32] Yu, Q., Tao, Z., Gao, X., Yang, Y.F., Han, L.H and Zhuang, J.P. *Research on Seismic Performance of FRP-confined RC Columns with High Axial Load Ratios*, Fuzhou University, China (in Chinese); 2004.

Table 1 Properties of columns in Fig. 4

Specimen	f_{cu} (MPa)	$f_{y,k}$ (MPa)	ρ_s (%)	h'/h	e_1/e_2	e_2/h	l/h
Column 1						0.5	15
Column 2	31 (13.8)	414 (360)	6	0.7	0	0.5	25
Column 3						0.1	40
Column 4						0.5	40

Table 2 Summary of Kim and Yang's tests

Specimen	b (mm)	h (mm)	f_{co}' (MPa)	f_y (MPa)	ρ_s (%)	l/h	h'/h	e_1/e_2	e_2/h	$N_{u,test}$ (kN)	$N_{u,theo}$ (kN)	$\dfrac{N_{u,theo}}{N_{u,test}}$
60L2-1	80	80	25.5	387	1.98	18	0.625	1	0.3	63.7	65.8	1.03
60L2-2										65.7		1.00
100L2-1						30				38.2	36.6	0.96
100L2-2										35.0		1.05
60M2-1	80	80	63.5	387	1.98	18	0.625	1	0.3	102.8	111.1	1.08
60M2-2										113.5		0.98
100M2-1						30				45.2	55.1	1.22
100M2-2										47.6		1.16
60H2-1	80	80	86.2	387	1.98	18	0.625	1	0.3	122.1	134.7	1.10
60H2-2										123.7		1.09
100H2-1						30				54.3	63.3	1.17
100H2-2										54.9		1.15

Note: ρ_s is the volumetric ratio of longitudinal steel reinforcement, and $N_{u,test}$ and $N_{u,theo}$ are the experimental and theoretical axial load capacities of a column, respectively.

Table 3 Summary of Ranger and Bisby's tests

Specimen	D (mm)	l (mm)	$\dfrac{e_1}{e_2}$	e_2 (mm)	Concrete Cover (mm)	E_{frp} (GPa)	t (mm)	f_{co}' (MPa)	f_y (MPa)	ρ_s (%)	$N_{u,test}$ (kN)	$N_{u,theo}$ (kN)	$\dfrac{N_{u,theo}}{N_{u,test}}$
U-0	152	600	1	0	25	90	0	33.2	710	0.71	497	641	1.29
C-0						90	0.381				873	786	0.90
U-5	152	600	1	5	25	90	0	33.2	710	0.71	459	584	1.27
C-5						90	0.381				770	725	0.94
U-10	152	600	1	10	25	90	0	33.2	710	0.71	447	525	1.17
C-10						90	0.381				664	655	0.99
U-20	152	600	1	20	25	90	0	33.2	710	0.71	351	420	1.20
C-20						90	0.381				579	518	0.89
U-30	152	600	1	30	25	90	0	33.2	710	0.71	253	322	1.27
C-30						90	0.381				337	402	1.19
U-40	152	600	1	40	25	90	0	33.2	710	0.71	179	242	1.35
C-40						90	0.381				264	305	1.16

Table 4 Summary of Fitzwilliam and Bisby's tests

Specimen	D (mm)	l (mm)	$\dfrac{e_1}{e_2}$	e_2 (mm)	Concrete Cover (mm)	E_{frp} (GPa)	t (mm)	$f_{co}^{'}$ (MPa)	f_y (MPa)	ρ_s (%)	$N_{u,test}$ (kN)	$N_{u,theo}$ (kN)	$\dfrac{N_{u,theo}}{N_{u,test}}$
300U-A	152	300	1	20	25	90	0	35.5	710	0.71	471	458	0.98
300U-B											462		
300C-1-0-A	152	300	1	20	25	90	0.381	35.5	710	0.71	675	531	0.78
300C-1-0-B											679		
300C-2-0-B	152	300	1	20	25	90	0.762	35.5	710	0.71	911	684	0.75
600U-A	152	600		20	25	90	0	35.5	710	0.71	428	448	1.05
600C-1-0-A	152	600	1	20	25	90	0.381	35.5	710	0.71	563	505	0.90
900U-A	152	900	1	20	25	90	0	35.5	710	0.71	398	432	1.09
900C-1-0-A	152	900	1	20	25	90	0.381	35.5	710	0.71	549	468	0.85
1200U-A	152	1200	1	20	25	90	0	35.5	710	0.71	389	411	1.03
1200U-B											411		
1200C-1-0-A	152	1200	1	20	25	90	0.381	35.5	710	0.71	451	433	0.93
1200C-1-0-B											481		
1200C-2-0-A	152	1200	1	20	25	90	0.762	35.5	710	0.71	539	466	0.86

Table 5 Cylinder tests in Fitzwilliam and Bisby and Ranger and Bisby

Source	$f_{co}^{'}$ (MPa)	E_{frp} (GPa)	t (mm)	$f_{cc}^{'}$ (MPa)	ε_{cu} (%)	$\varepsilon_{h,rup}$ (%)	$f_{cc}^{'}$-predicted (MPa)	ε_{cu}-predicted (%)
Fitzwilliam and Bisby	34.6	90	0.381	41	0.804	1.140	46.0	1.24
				39.7	0.768	1.165		
				41.4	0.793	1.192		
	35.8	90	0.762	59.8	0.165	1.111	63.9	1.76
	36.4	90	0.762	58	0.112	1.175	65.6	1.83
				62.5	0.156	1.151		
Ranger and Bisby	33.2	90	0.381	44.2	0.860	1.15	44.7	1.25

Table 6 Summary of Tao *et al.*'s tests

Specimen	D (mm)	l (mm)	$\dfrac{e_1}{e_2}$	e_2 (mm)	Concrete Cover (mm)	f_{co}' (MPa)	f_y (MPa)	ρ_s (%)	E_{frp} (GPa)	t (mm)	$N_{u,test}$ (kN)	$N_{u,theo}$ (kN)	$\dfrac{N_{u,theo}}{N_{u,test}}$
C1-1U	150	1260	1	0	21	48.2	388.7	2.56	255	0.34	455	942(658)	2.07(1.45)
C1-1R											765	1018(871)	1.33(1.14)
C1-2U	150	1260	1	50	21	48.2	388.7	2.56	255	0.34	149	273(198)	1.83(1.33)
C1-2R											248	288(243)	1.16(0.98)
C1-3U	150	1260	1	100	21	48.2	388.7	2.56	255	0.34	88	119(101)	1.35(1.15)
C1-3R											124	131(119)	1.06(0.96)
C1-4U	150	1260	1	150	21	48.2	388.7	2.56	255	0.34	54.5	75.9(68.6)	1.39(1.26)
C1-4R											77	79.5(75.0)	1.03(0.97)
C2-1U	150	3060	1	0	21	48.2	388.7	2.56	255	0.34	276	668(392)	2.42(1.42)
C2-1R											386	700(543)	1.81(1.41)
C2-2U	150	3060	1	50	21	48.2	388.7	2.56	255	0.34	108	146(114)	1.35(1.06)
C2-2R											126	149(131)	1.18(1.04)
C2-3U	150	3060	1	100	21	48.2	388.7	2.56	255	0.34	62.5	76.1(67.4)	1.22(1.08)
C2-3R											71.5	77.6(72.9)	1.08(1.02)
C2-4U	150	3060	1	150	21	48.2	388.7	2.56	255	0.34	39	54.0(49.7)	1.83(1.27)
C2-4R											47.5	55.1(52.8)	1.16(1.11)
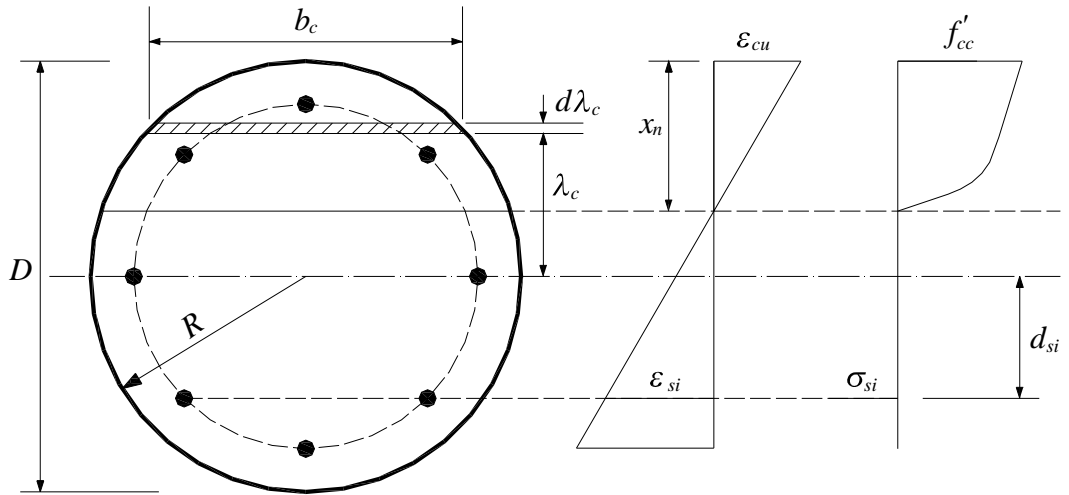
Fig. 1 Strains and stresses over an FRP-confined circular RC section
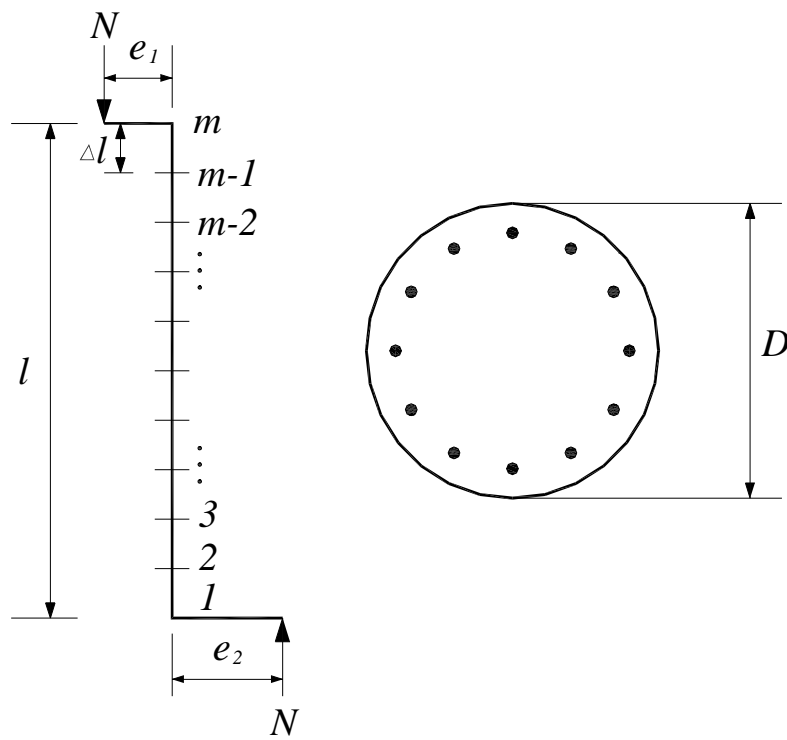
Fig. 2 Schematic of the theoretical model
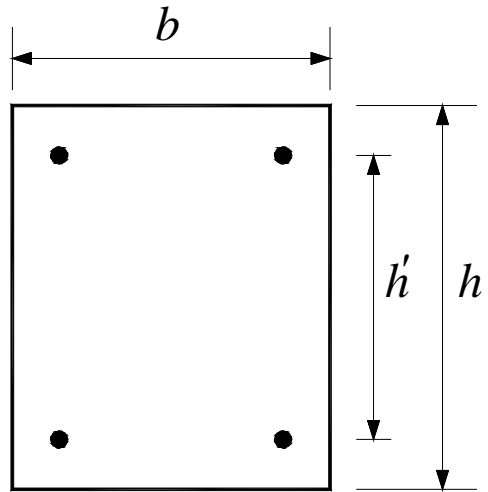
Fig. 3 Cross section of the columns considered in Fig. 4
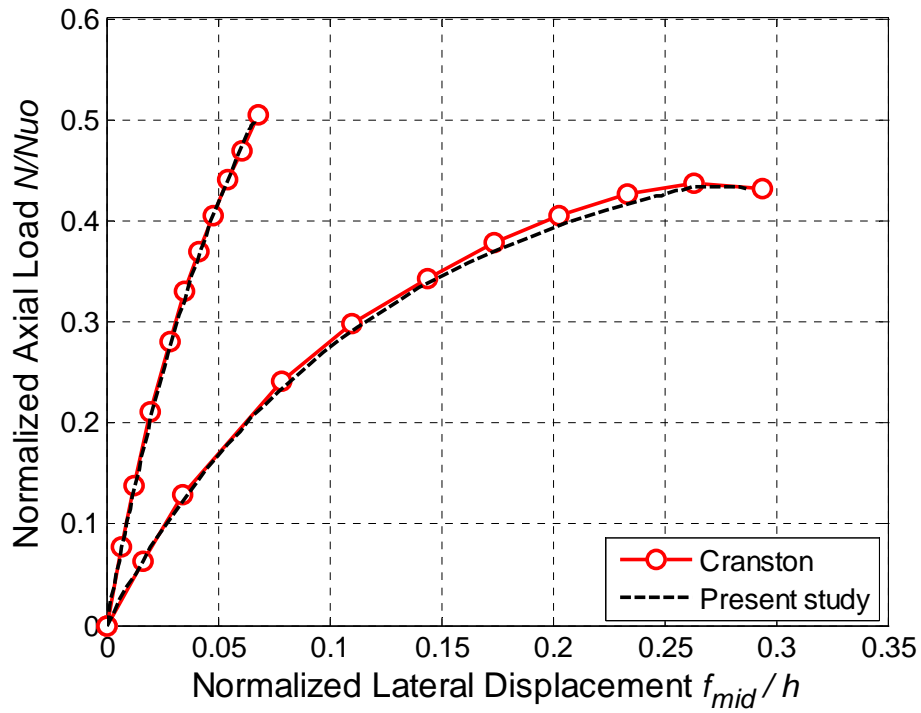
(a) Columns 1 and 2
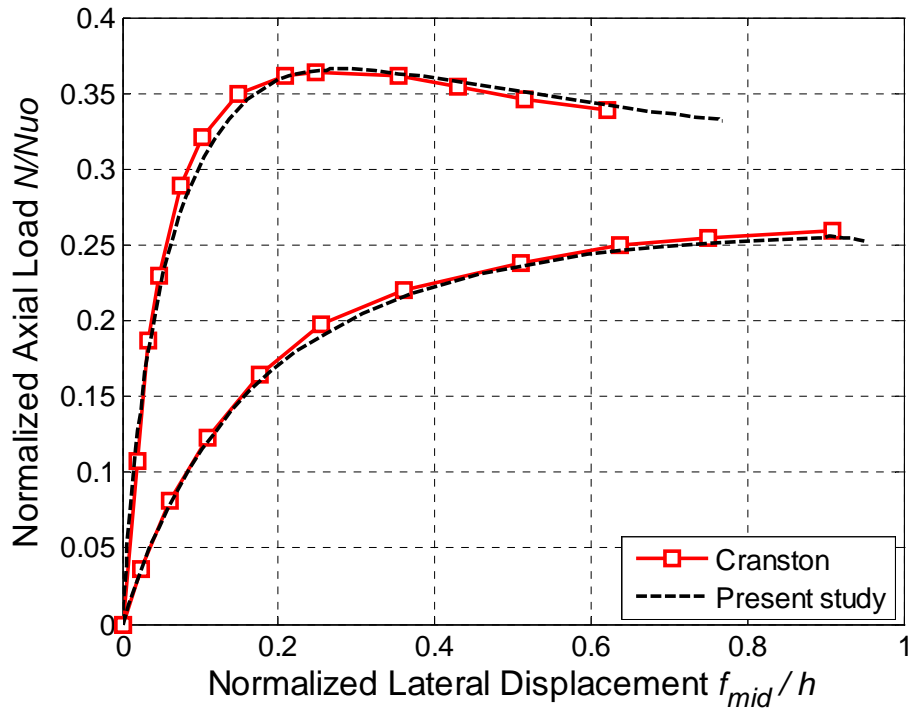
(b) Columns 3 and 4

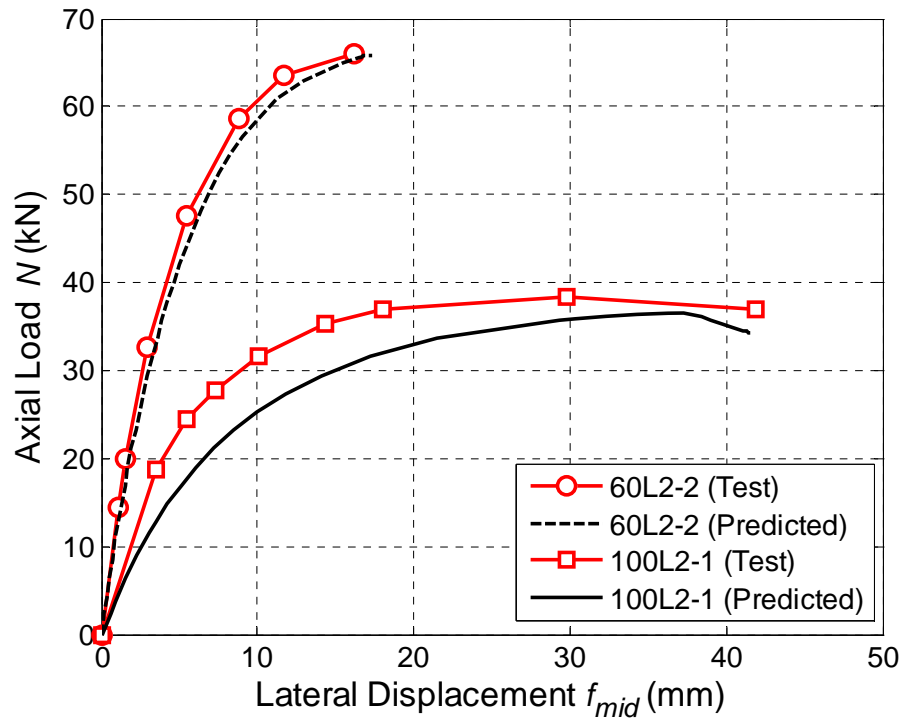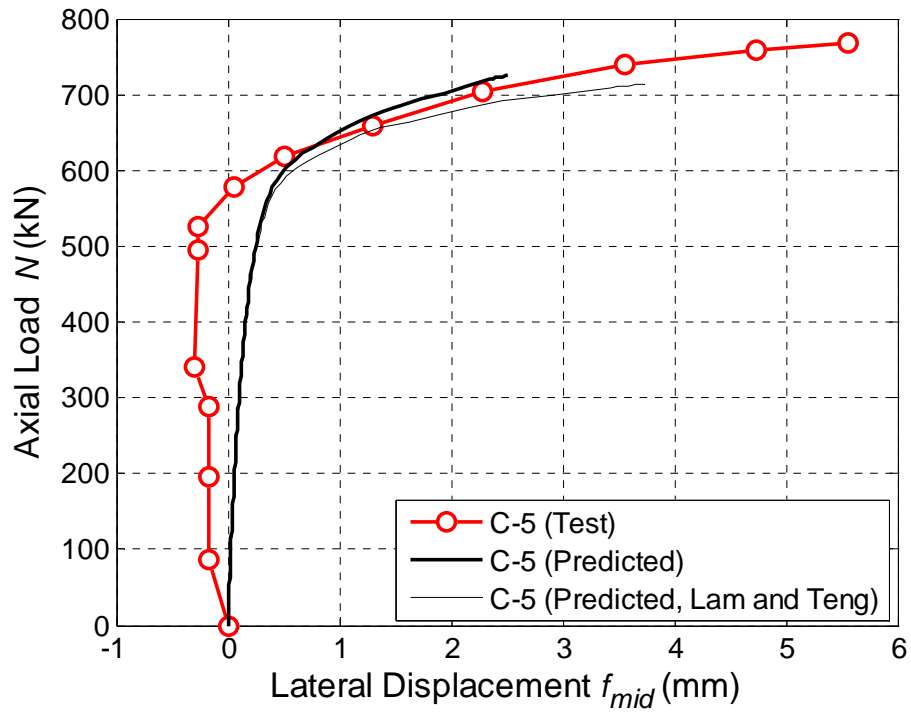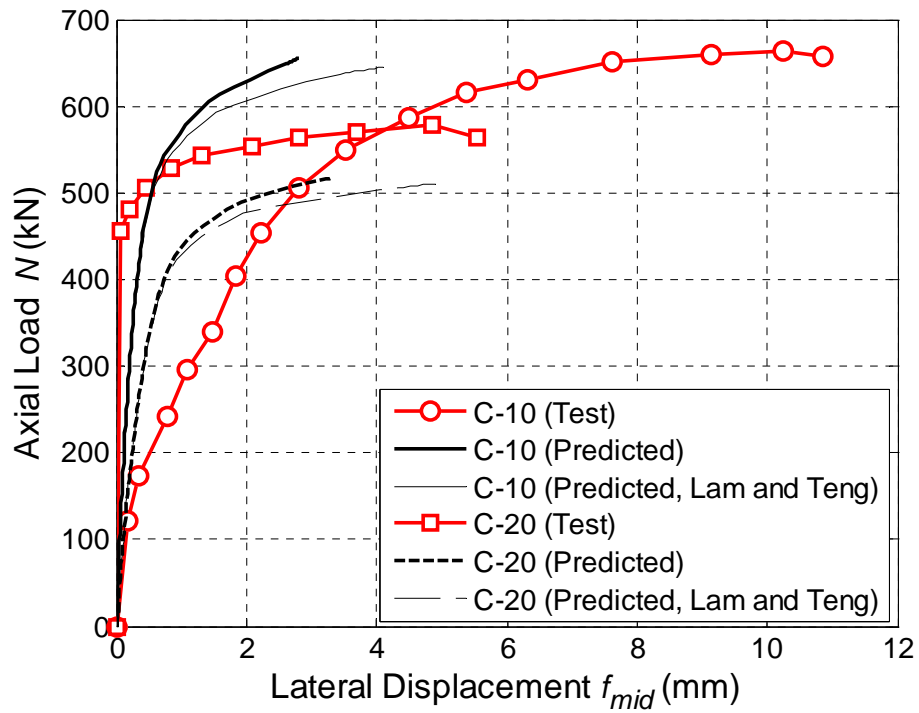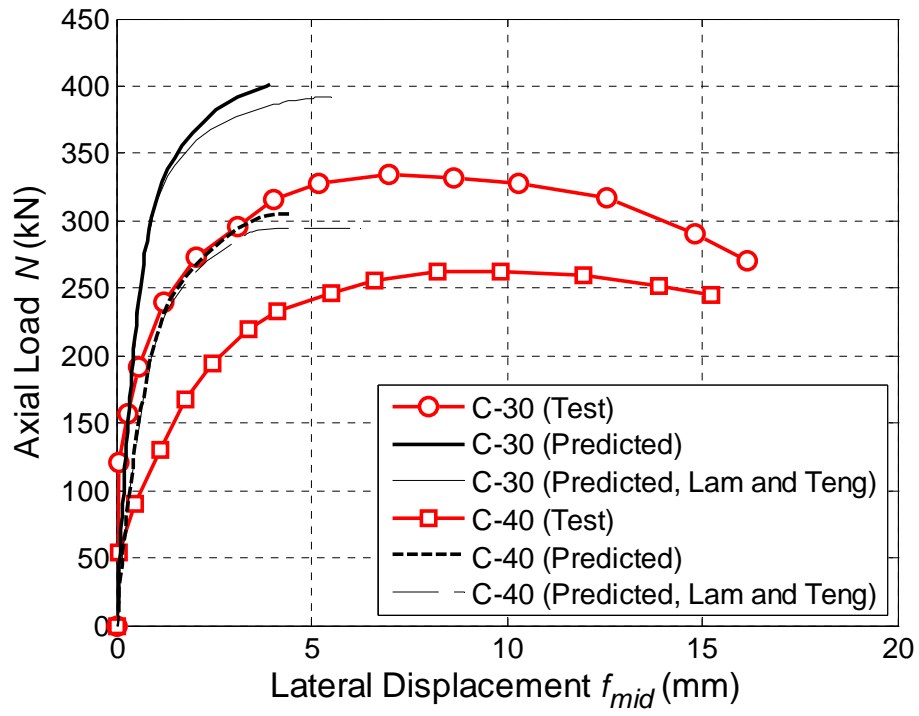Fig. 4 Comparisons with Cranston's theoretical model
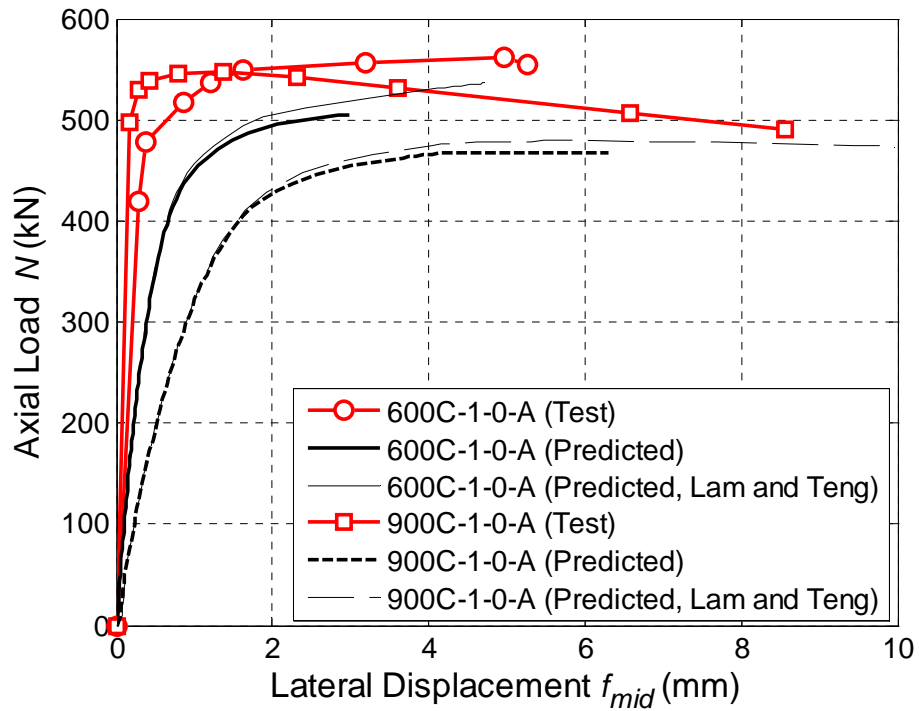
Fig. 5 Comparisons with Kim and Yang's tests

(a) Column C-5

(b) Columns C-10 and C-20

(c) Columns C-30 and C-40

Fig. 6 Comparison with Ranger and Bisby's tests

(a) Columns 600C-1-0-A and 900C-1-0-A
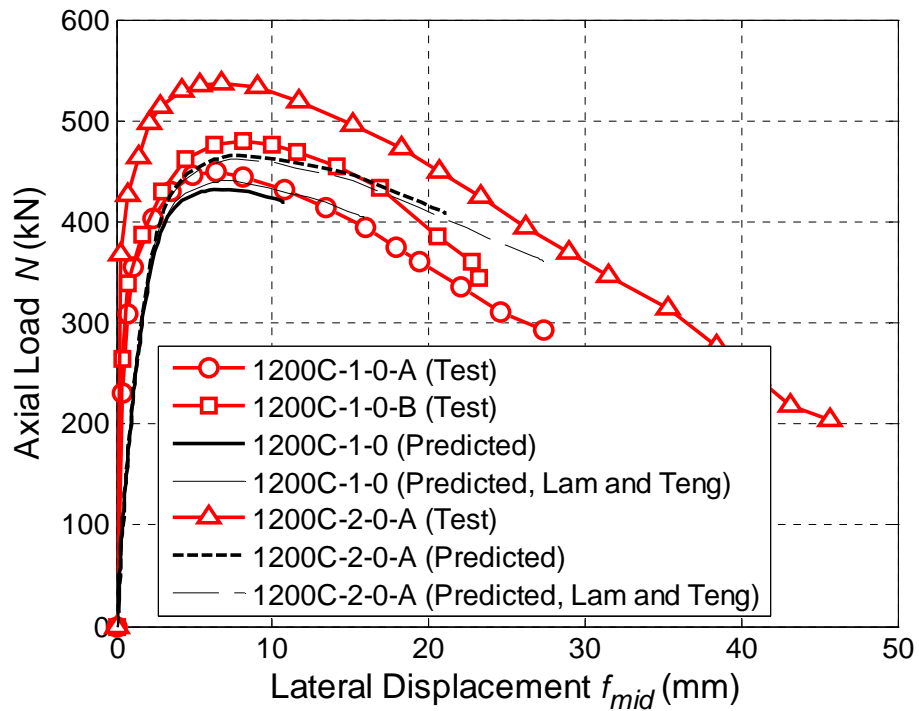
(b) Columns 1200C-1-0-A, 1200C-1-0-B and 1200C-2-0-A
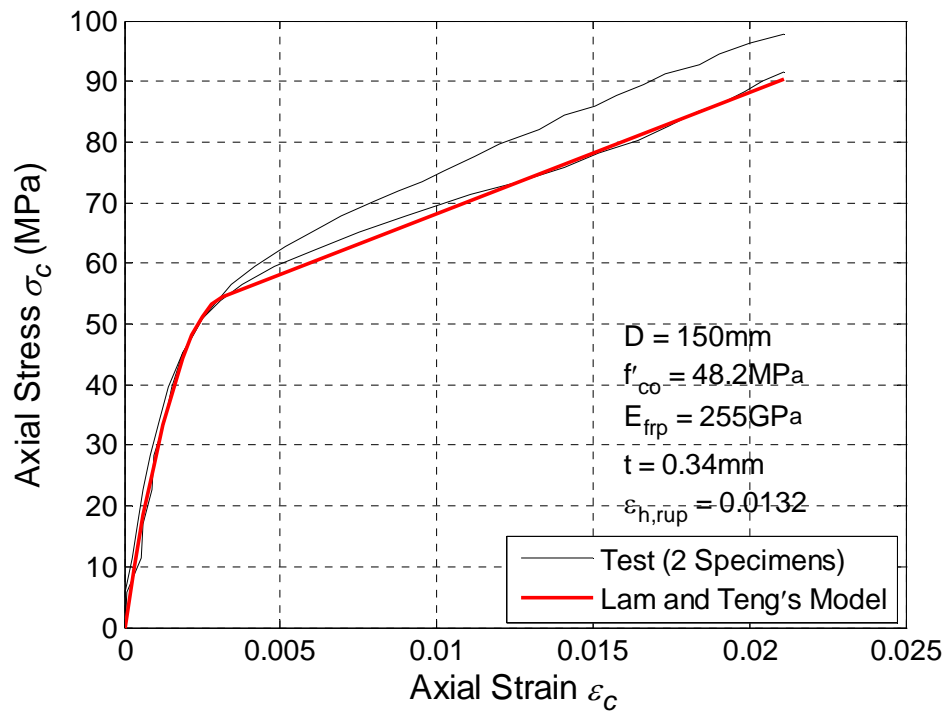
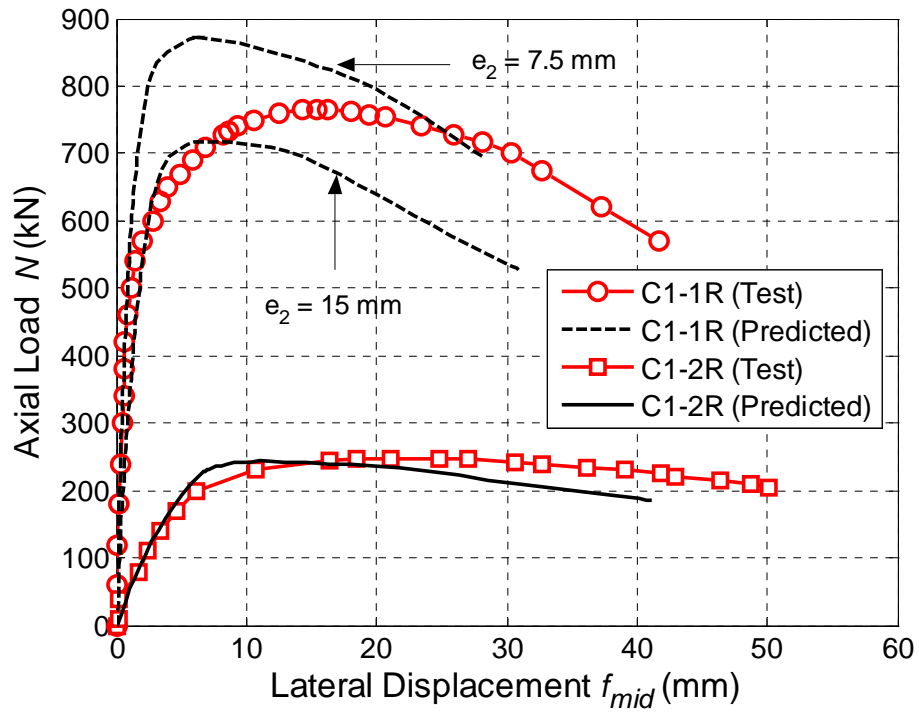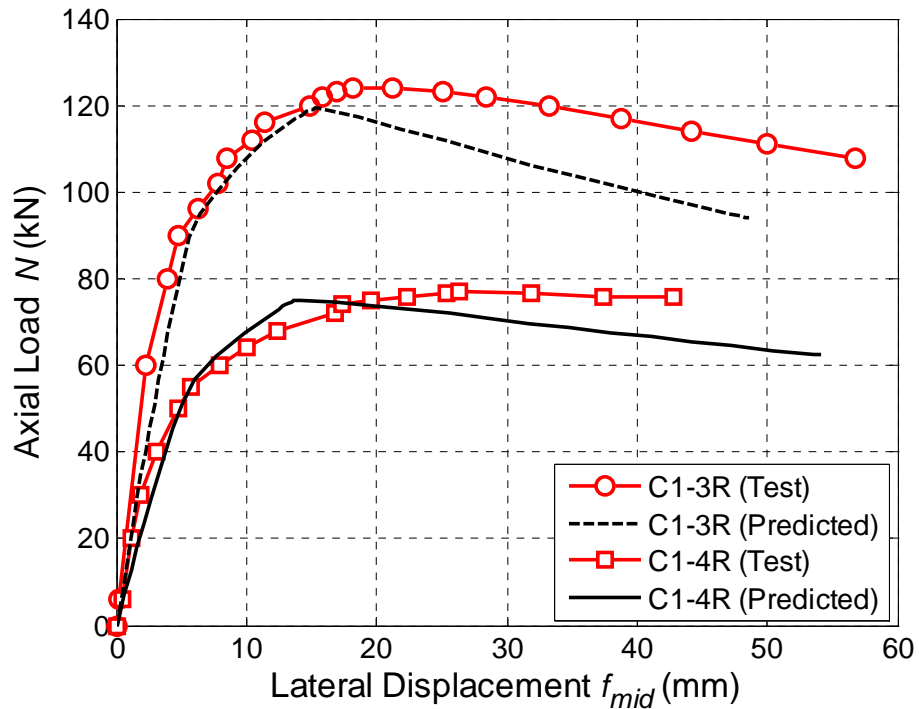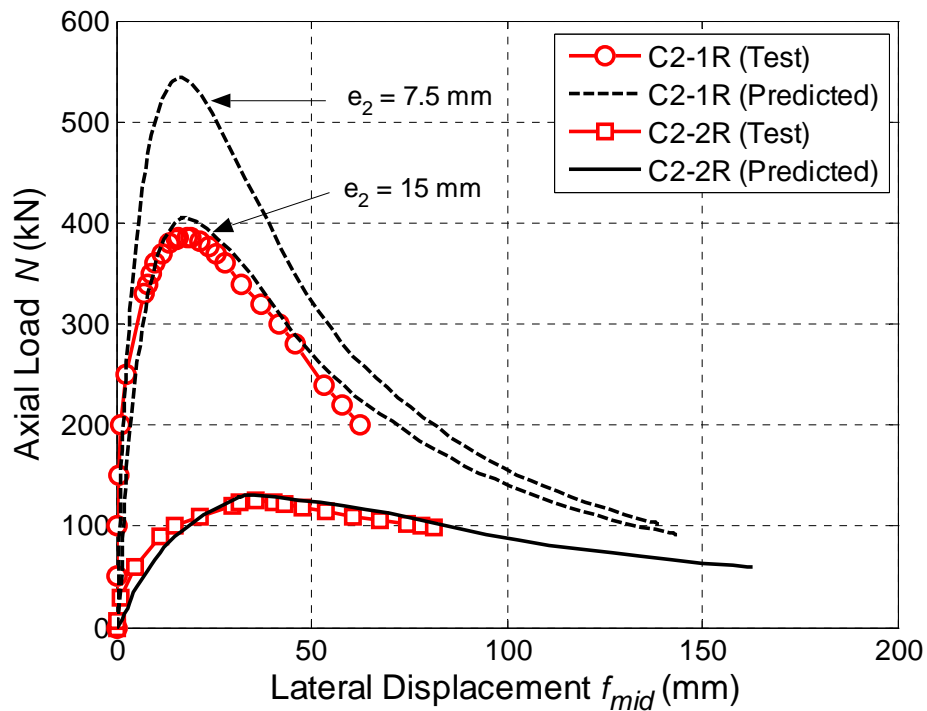Fig. 7 Comparison with Fitzwilliam and Bisby's tests

Fig. 8 Comparison with Tao *et al.*'s cylinder tests

The chart shows Axial Stress σ_c (MPa) on the y-axis ranging from 0 to 100, and Axial Strain ε_c on the x-axis ranging from 0 to 0.025.

Chart parameters:
D = 150mm
f'_{co} = 48.2MPa
E_{frp} = 255GPa
t = 0.34mm
$\varepsilon_{h,rup}$ = 0.0132

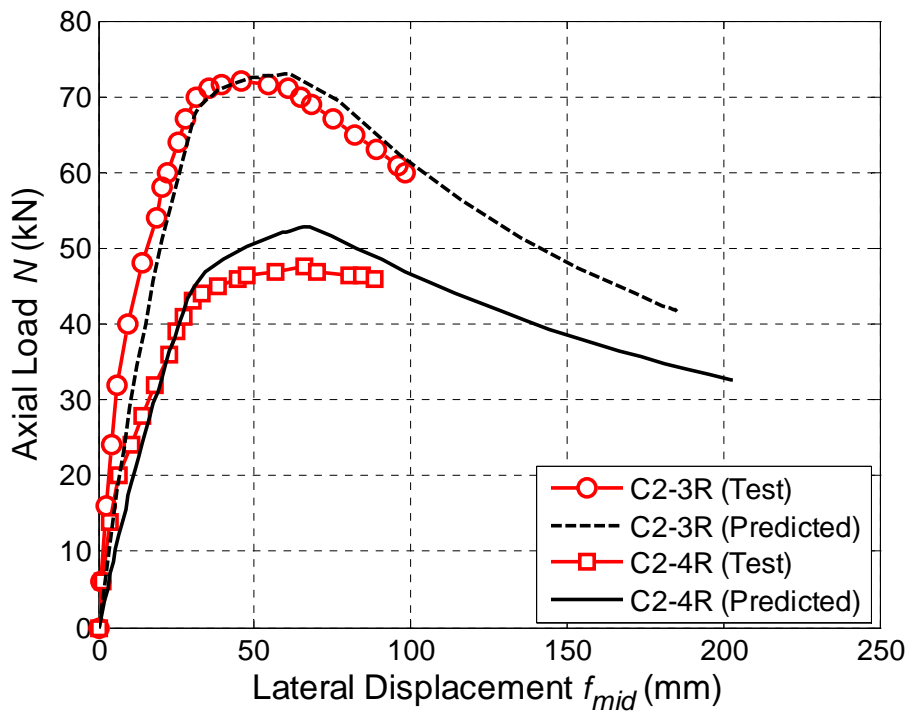Legend:
Test (2 Specimens)
Lam and Teng's Model

(a) Columns C1-1R and C1-2R

(b) Columns C1-3R and C1-4R

(c) Columns C2-1R and C2-2R

(d) Columns C2-3R and C2-4R

Fig. 9 Comparisons with Tao *et al.*'s tests on FRP-confined RC columns